Characterisation of homologous sphingosine 1-phosphate lyase (S1PL) isoforms in the bacterial pathogen *Burkholderia pseudomallei*

Christopher McLean[1], Jon Marles-Wright[2#], Rafael Custodio[3], Jonathan Lowther[1], Amanda J. Kennedy, Jacob Pollock[1], David J. Clarke[1], Alan R. Brown[3], Dominic J. Campopiano[1*]

1 EastChem School of Chemistry, David Brewster Road, The University of Edinburgh, Edinburgh, EH9 3FJ, UK.

2 Institute of Quantitative Biology, Biochemistry and Biotechnology, School of Biological Sciences, The University of Edinburgh, Max Born Crescent, Edinburgh, EH9 3BF, UK.

3 Geoffrey Pope Building, University of Exeter, Stocker Road, Exeter, EX4 4QD, UK.

***** To whom correspondence should be addressed. Email Dominic.Campopiano@ed.ac.uk

Current address:

School of Biology, Newcastle University. Newcastle upon Tyne, NE1 7RU.

Abstract

Sphingolipids (SLs) are ubiquitous elements in eukaryotic membranes and are also found in some bacterial and viral species. As well as playing an integral structural role, SLs also act as potent signalling molecules involved in numerous cellular pathways and have been linked to many human diseases. A central SL signalling molecule is sphingosine-1-phosphate (S1P) whose breakdown is catalysed by sphingosine-1-phosphate lyase (S1PL), a pyridoxal 5'-phosphate (PLP) dependent enzyme that catalyses the cleavage of S1P to (*2E*)-hexadecenal (2E-HEX) and phosphoethanolamine (PE). Here we show the pathogenic bacterium *Burkholderia pseudomallei* K96243 encodes two homologous proteins (S1PL2021 and S1PL2025) that display moderate sequence identity to known eukaryotic and prokaryotic S1PLs. Using an established mass spectrometry-based methodology we show that recombinant S1PL2021 is catalytically active. Also, we used recombinant human fatty aldehyde dehydrogenase (FALDH) to develop a spectrophotometric, enzyme-coupled assay to detect 2E-HEX formation and measure the kinetic constants of the two *B. pseudomallei* S1PL isoforms. Furthermore, we determined the x-ray crystal structure of the PLP-bound form of S1PL2021 at 2.1 Å resolution revealing the enzyme displays a conserved structural fold and active site architecture comparable with known S1PLs. The combined data suggest that *B. pseudomallei* has the potential to degrade host SLs in a S1PL-dependent manner.

Keywords

Sphingolipids, sphingosine-1-phosphate lyase, pyridoxal 5'-phosphate, assay, fatty aldehyde dehydrogenase, *Burkholderia*

Abbreviations: SLs, sphingolipids; S1P, sphingosine-1-phosphate; S1PL, sphingosine-1-phosphate lyase; PLP, pyridoxal 5'-phosphate; FALDH, fatty aldehyde dehydrogenase; 2E-HEX, (*2E*)-hexadecenal, PE, phosphoethanolamine; PDB, Protein Data Bank; ESI-MS, electrospray ionisation mass spectrometry.

Introduction

Sphingolipids (SLs) are a diverse family of natural metabolites composed of a fatty acyl chain attached to a polar headgroup derived from L-serine that together form the sphingoid base core (1). Amphipathic in nature, SLs are important structural components of eukaryotic membranes that can associate with each other and with other membrane components (such as cholesterol and proteins) in regions called lipid rafts (2). As well as this structural role, SLs are now recognised as fundamental signalling molecules with a vast array of functions within cells. A 'sphingodynamics' model has been proposed to encompass both intra and extracellular signalling by all bioactive SL intermediates and their metabolites (3). Sphingosine-1-phosphate (S1P) is one such SL that regulates a plethora of physiological processes in humans by activating five different G-protein coupled S1P receptors (named S1PRs 1-5) (4). Perturbing the cellular levels of S1P can have serious consequences and has been linked to diseases such as cancer, diabetes, atherosclerosis, osteoporosis and neurodegeneration (5, 6). The balance between S1P and ceramide, another signalling molecule that often has opposing cellular effects to S1P, is governed by a 'sphingolipid rheostat' (6, 7). Remarkably, the pyridoxal 5′-phosphate (PLP) dependent enzyme sphingosine-1-phosphate lyase (S1PL) is the only known enzyme capable of irreversibly removing sphingoid bases from the SL pool. S1PL catalyses the retro-aldol like breakdown of S1P to 2E-hexadecenaldehyde (2E-HEX) and phosphoethanolamine (PE) (Fig. 1). In eukaryotes the 2E-HEX is oxidised by fatty aldehyde dehydrogenase (FALDH, also known as ALDH3A2) to the hexadecenoic acid which links the SL and glycerol phospholipid metabolic pathways (8). Saba and Hannun were the first to clone a S1PL gene (also known as *dpl1* and *BST1*) from *Saccharomyces cerevisiae* in 1997 (9) and subsequently the human homologue was characterised in 2000 (10). Since S1P plays a role in numerous diseases, enzymes in the S1P biosynthetic and degradative pathways are now seen as attractive drug targets(3). To that end, Novartis recently published results of a medicinal chemistry study that identified potent and specific inhibitors of human S1PL (11).

Nearly all Gram negative bacteria such as *Escherichia coli*, *Legionella pneumophila* and *Burkholderia pseudomallei* contain lipopolysaccharides (LPS) as the major lipid component in their cell membranes. In contrast, the number of bacteria that produce SLs, examples being *Sphingomonas spp.*(12) and *Myxobacterium spp.* (13), is relatively small. However, it is interesting to note that many of the bacteria that are part of the human microbiome such as *Bacteroides fragilis* and *Porphyromonas gingivalis* also produce SLs (14–16). This

raises the interesting question of what is the function of bacterial SLs? Moreover, if such species contain an S1PL enzyme, what role does it play in bacterial metabolism in general and in the host-microbe interaction in particular? Recent studies have begun to address these questions. A bacterial S1PL homologue (LegS2) was identified in the intracellular human pathogen *L. pneumophila* (17, 18) and its role as a virulence factor in the pathogenic mechanism of this organism was explored. *B. pseudomallei* is an intracellular Gram negative pathogen that causes serious disease in humans and animals and as such, is classified by the Centre for Disease Control (CDC) as a category B biothreat agent. *B. pseudomallei* infection results in melioidosis, a febrile and potentially fatal disease which has a high mortality rate (19). To date, there have been no studies on SL metabolism in *Burkholderia*, so we began by investigating if this species contains any of the known SL metabolic enzymes and the recent work on the *L. pneumophila* focussed our attention on S1PL. We searched the *B. pseudomallei* K96243 genome (20, 21) and surprisingly, found two ORFs *BPSS2021* and *BPSS2025*, whose gene products (S1PL2021 and S1PL2025 respectively) displayed high sequence identity to each other and moderate sequence conservation to confirmed S1PLs from bacteria, yeast and humans. We felt this unusual gene duplication merited further study, thus we set out to characterise the biochemical properties of these putative *B. pseudomallei* S1PLs as a prelude to investigating their role in the host-pathogen interaction.

A number of assays that monitor S1PL activity have been reported in the literature. Many use either radioactive (e.g. ^{3}H or ^{14}C) or fluorescently-labelled (e.g. BODIPY) S1P analogues that generate labelled 2E-HEX aldehyde that can be detected by scintillation counting or fluorescent methods respectively (22–25). Other assays rely on the chemical derivatization of the HEX aldehyde product using chemical reagents, then applying mass spectrometry (MS) to quantify the amount of material (LC-ESI-MS/MS, GC-MS, HPLC-ESI-QTOF *etc*) (26–28). Each approach has its merits with respect to sensitivity, limit of detection and the ability to work with purified enzyme, cell-free extracts or in whole cells. However, the drawbacks include the use of radioactive or non-natural substrates, limited throughput and the requirement for the extraction of the S1PL reaction products. First, using an established MS-based methodology we validated that the recombinant S1PL2021 displayed S1PL activity (26). Then, to further characterise the two closely-related *B. pseudomallei* S1PLs we generated a coupled spectrophotometric method for the convenient measurement of S1PL activity. This assay couples the activity of these new S1PLs with a recombinant form of human fatty aldehyde dehydrogenase (FALDH) that is part of the 2E-HEX catabolic pathway. In this way we were able to measure the production of 2E-HEX via the

reduction of the FALDH NAD^+ cofactor to NADH. Furthermore, we determined the X-ray crystal structure of the S1PL2021 isoform at 2.1 Å and revealed that it has features in common with bacterial, yeast and human S1PL homologs. As well as reporting a convenient assay for S1PL activity, this study lays the foundation for future studies of the role of these novel S1PLs in the growth and pathogenicity of *Burkholderia*.

MATERIALS AND METHODS

Materials

Plasmids and *E. coli* competent cells for cloning were purchased from Novagen and New England Biolabs. The *E. coli* BL21 (DE3) competent cells used for protein expression were from Agilent. All chromatography columns were from GE Healthcare. Hotstart *Pfu* polymerase was from Agilent. Restriction enzymes were from New England BioLabs. Oligonucleotide primers were sourced from Sigma. Substrate S1P (CAS No. 26993-30-6) was from Cayman Chemical Company. (*2E*)-hexadecenal (2E-HEX) was synthesized in house using a published method (29). All other buffers and reagents were sourced from Sigma.

Sequence alignment and prediction tools

Sequence data searches were performed using the BLAST suite of programs. Multiple sequence alignments were carried out using the Clustal series of programs (30) with structural modelling performed using the Phyre2 server (31). To find S1PL homologs in the curated *B. pseudomallei* genome (www.burkholderia.com) the S1PL sequence from *Symbiobacterium thermophilim* (Uniprot: Q67PY4, PDB: 3MAU) was used to carry out a standard BLAST analysis. This recovered two hit genes, annotated as *BPSS2021* (Uniprot: Q63IP8) and *BPSS2025* (Uniprot: Q63IP4) with moderate sequence identities to the template (43 and 44% respectively). The encoded proteins, referred to as S1PL2021 and S1PL2025 share ~86% sequence identity.

Cloning and expression of *BPSS2021* (S1PL2021)

Sequence analysis suggested that the *BPSS2021* gene could be expressed from two start codons to give two open reading frames (ORFs). Therefore, PCR forward and reverse primers were designed based on the longest ORF (S1PL2021 N-EXT) using the following primers:

S1PL2021 forward 5' ***CCATGG***TGCGTTCGATCGC 3'

S1PL2021 reverse 5' ***CTCGAG***CGGACAGTCGGTAAACAG 3'

These primers incorporated NcoI and XhoI restriction sites giving a C-terminal six-histidine tagged fusion. A positive pGEM/ S1PL2021 N-EXT clone was digested and the isolated S1PL gene ligated into pET-28a. This gave a pET-28a/S1PL2021 N-EXT construct that expressed a protein of 500 aa. To clone the shorter ORF (S1PL2021), a forward primer was designed to initiate expression from an ***ATG*** start codon 60 base pairs downstream of the annotated start codon;

S1PL2021 TRUNC forward: 5' ***CCATGG***ATCTCGAAGAAGG 3'.

This PCR product was also cloned into pET-28a via a pGEM intermediate to give a pET-28a/S1PL2021plasmid encoding a protein of 480 aa. Plasmids pET-28a/S1PL2021 N-EXT and pET-28a/S1PL2021 were used to transform *E. coli* BL21 (DE3) competent cells and selection was carried out on agar plates containing kanamycin (30 µg/ml, LB/Kan^{30}). Single colonies were used to inoculate 2x250 ml of LB/Kan^{30} broth and overnight cultures were grown at 37 °C with shaking at 250 rpm. The overnight cultures were used to inoculate 4l of fresh LB/Kan^{30} broth and grown to an A_{600} of 0.6-0.8. Protein expression was induced by addition of IPTG to a final concentration of 0.1 mM and growth was continued for 5 h at 30°C. Cells were harvested by centrifugation (Sorvall RC5-B centrifuge) at 5000 rpm for 15 minutes at 4°C.

Cloning and expression of the S1PL2021 K271A mutant

S1PL2021C mutants were prepared using the method of Naismith and Liu with primers were designed to introduce the relevant mutations (32).

K271A forward 5'CGATACGCAC***GCG***TTCGGCTACGGCCCGAAGGGC3'

K271A reverse 5'CGCCCTTCGGGCCGTAGCCGAA***CGC***GTGCGTATCG3'

PCR reactions were set up using Hotstart *Pfu* polymerase with completed reactions digested with Dpn1 enzyme to degrade template DNA. The post digestion mixture was transformed into high cloning efficiency cells (C2987- New England Biolabs) and spread on LB/Kan^{30} plates. Colonies were picked into LB/Kan^{30} and grown overnight with plasmid DNA extracted from cells using a Qiaprep miniprep kit (Qiagen). Sequencing was

performed to ensure mutagenesis had occurred. Expression of the S1PL2021 mutants mirrored that of the wildtype with the exception that induction temperature was reduced to 28°C.

Cloning and expression of *BPSS2025* (S1PL2025)

The coding sequence for the *BPSS2025* gene was amplified from *B. pseudomallei* K96243 chromosomal DNA using primers:

S1PL 2025 forward: 5' ***CCATGG***ATCTGGAGGAAGGCATCAG 3'

S1PL 2025 reverse 5' ***CTCGAG***AAGCGGGCAATCCGTGAAC 3'

to give an expressed protein sequence that aligned with the shorter S1PL2021 form described above. The purified PCR product was cloned into the pGEM T-Easy vector by TA ligation and positive clones were isolated and sequenced to confirm the identity of the gene. A positive pGEM/S1PL2025 clone was digested with NcoI and XhoI and the isolated S1PL gene ligated into pET-28a to give a C-terminally six His-tag protein of 480 aa. Expression of the gene and purification of the protein product was essentially identical to that for S1PL2021.

Cloning and expression of full length and truncated FALDH

The full length FALDH gene sequence (coding isoform 2) was purchased as a cDNA clone from Imagenes in a pOTB7 vector (Uniprot: P51648). Full length FALDH (isoform 1 and 2) is predicted to contain a C-terminal, membrane-bound helix thus using this as a template, full length and truncated versions for the FALDH isoform 1 (the major natural form) coding sequences were amplified by PCR using forward and reverse primers with NdeI/NcoI and XhoI restriction enzyme sites.

FALDH forward: 5' ***CATATG***GAGCTCGAAGTCCGGCGGGTCCGACAGG.

FALDH reverse: 5' ***CTCGAG***(TCA)TAATATTCCGCCTTGACAAGCACAGCGGCTACAAT.

Truncated FALDH reverse: 5' ***CTCGAG***ATCCACCTTTGACTGGCTGTTGGG.

The purified PCR products were cloned into pGEM, sequenced verified, and then cloned into pET-28a as described for the S1PL constructs as an N-terminally hexa-his tagged protein. pET-28a plasmids containing

both versions of FALDH (full length and C-terminal truncation) were used to transform *E. coli* BL21 (DE3) competent cells and selection was carried out on LB/Kan^{30} plates. Single colonies were used to inoculate 2x250 ml of LB/Kan^{30} broth and overnight cultures were grown at 37 °C with shaking at 250 rpm. The overnight cultures were used to inoculate 4.5l of fresh LB/Kan^{30} broth and grown to an A_{600} of 0.6-0.8. Protein expression was induced by addition of IPTG to a final concentration of 0.1 mM and growth was continued for 5 h at 22 °C. Cells were harvested by centrifugation (Sorvall RC5-B centrifuge) at 5000 rpm for 15 minutes at 4°C.

General procedure for the purification of six his-tagged enzymes (S1PL2021, S1PL2025 and FALDH)

All purification steps were carried out at 4°C. All buffers contained 2 0mM HEPES (pH 7.5), 400 mM NaCl and 10% glycerol. 100 µM PLP was included in the buffer for S1PL isolation. Binding buffers also contained 10 mM imidazole and one EDTA-free protease inhibitor tablet (Roche). Wash buffer contained 30 mM imidazole with elution buffer containing 300 mM imidazole. Cell pellets (~4 g) were resuspended in Ni-NTA binding buffer 10:1 (v/w). Cells were lysed by sonication (Soniprep 150) for 15 cycles (30s on, 30s off) on ice. In the case of full length FALDH, 0.1% N-lauroylsarcosine was added to aid solubilisation of the recombinant protein. The lysed cell suspension was centrifuged at 20,000 rpm for 30 minutes. The cell-free extract was filtered (0.45µm syringe filter) before addition of 2 ml Ni-NTA resin (Qiagen) pre-equilibrated with binding buffer. Binding was carried out by rotating the suspension at 4°C for 1 hour. The resin was collected by gravity flow in a fritted plastic disposable column, washed with 30 ml wash buffer, and the bound protein eluted with 5 ml elution buffer. Fractions were analysed by SDS PAGE and the 300 mM imidazole eluate loaded onto a pre-equilibrated HiPrep™ 16/600 Superdex™ S-200 size exclusion column. Recombinant protein was eluted at a flow rate of 1 ml/min in buffer. The molecular weights of S1PL or FALDH were calculated from a calibration curve using known molecular mass standards (GE Healthcare). The purity of the recombinant proteins were analysed by SDS PAGE. The fractions were pooled and protein concentration was calculated by A_{280} using the relevant extinction coefficients as determined using the Scripps Protein Calculator.

S1PL UV-visible spectroscopy

All UV-visible spectra were recorded on a Cary 50 spectrophotometer (Varian) and analysed using Cary WinUV software (Varian). S1PL enzymes (15-20 µM) were maintained in holo-form by dialysing against buffer containing 20 mM HEPES (pH 7.5), 400 mM NaCl, 10% glycerol and 100 µM PLP. Prior to spectroscopic measurements excess PLP was removed using a PD-10 desalting column (GE Healthcare). A stock solution of S1P (1 mg/ml) was prepared in 1% triton X-100 and sonicated. A stock solution of phosphoethanolamine (PE, 100 mM) in water. S1P and PE were added to the enzymes and scans recorded between 300-500 nm at appropriate time intervals.

Assay of S1PL activity by LC/MS

The activity of S1PL was determined by detecting the formation of the (*2E*)-hexadecenal semicarbazone (2E-HEX SC) product by LC/MS using the method of Berdyshev *et al* (26). Briefly an enzyme stock solution was prepared by dialysing 10 µM S1PL in 20 mM HEPES (pH 7.5), 400 mM NaCl, and 100 µM PLP. A 2.6 mM S1P stock was prepared with additional sonication. Using these stocks an enzyme assay was prepared to a final volume of 500 µl containing 6 µM S1PL and 0.26 mM S1P substrate in a reaction buffer containing 20 mM HEPES, 400 mM NaCl and 0.1 mM PLP. Control assays were prepared accordingly and all samples were incubated for 20 minutes at 37°C with methanol then added to stop the reaction. The 2E-HEX was extracted and the semicarbazone derivative produced by heating reaction aliquots with 0.2 ml of 5 mM semicarbazide hydrochloride in methanol containing 5% formic acid at 40°C for 2 h. The semicarbazones were analysed by mass spectrometry with samples injected via an Agilent 1200 HPLC with interfaced auto-sampler (Agilent Technologies). Analysis was in ESI –positive mode on a micro-TOF2 (Bruker Daltonics) using a standard ESI source. Ion source conditions were as follows; the ESI voltage was held at 4.5 kV at a temperature of 200°C with a Hexapole RF of 70V peak to peak and skimmer 2 potential of 20V.

Assay of FALDH activity using UV-vis spectroscopy

The soluble version of FALDH, lacking its C-terminus, was assayed to determine its suitability as a coupling enzyme with S1PL. This was done by monitoring the formation of NADH in the presence of a synthetic 2E-HEX substrate. Reaction aliquots were prepared to a final volume of 500 µl containing 1 mM NAD^+, 500 nM

FALDH in a reaction buffer containing 20 mM HEPES (pH 7.5), 400 mM NaCl. Reactions were monitored by UV-Vis at 340nm for 30 minutes at 37°C. Subsequent assays were performed in a Synergy HT plate reader and the data plotted using GraphPad (non-linear regression analysis) to gain kinetic data for FALDH. The reaction was linear over ~5 minutes and the lower limit of detection was ~4 µM 2E-HEX.

S1PL:FALDH coupled-enzyme assay

S1PL enzyme assays were prepared to a final volume of 500 µl containing 6 µM S1PL, 1 mM NAD^+, 500 nM FALDH in a reaction buffer containing 20 mM HEPES (pH 7.5), 400 mM NaCl and 0.1 mM PLP. The reaction was initiated by the addition of S1P from the stock solution to give a final concentration of 400 µM. Control samples lacking enzyme or substrate were also prepared. Reactions were monitored by UV-Vis at 340nm for 30 minutes at 37°C on a spectrophotometer. For kinetic data the assays were then transferred to a Synergy HT plate reader and these contained 6 µM S1PL, 1 mM NAD^+, 500 nM FALDH in a reaction buffer containing 20 mM HEPES (pH 7.5), 400 mM NaCl and 0.1 mM PLP (final well volume 150 µl). This time substrate S1P (0-175 µM) was prepared in 1% triton X-100 and added to separate reaction aliquots in triplicate. Reactions were monitored at 340nm for 30 minutes at 37°C. Kinetic data was fit using GraphPad as described previously.

X-ray crystallography

S1PL2021 at 6 mg/ml was crystallised by hanging-drop vapour diffusion at 18°C. Crystallisation experiments were set up in 96 well MRC plates with commercially available screens from Molecular Dimensions Limited with 100 nl drops of protein and 100 nl well solution and equilibrated against 70 µl of well solution. Crystals grew in a well solution of 20% (v/v) polypropylene glycol 400, 10% (v/v) 1-propanol (Molecular Dimensions MIDAS screen). Crystals were cryoprotected with mineral oil and then flash cooled by immersion in liquid nitrogen. Datasets were collected on beamline I03 at the Diamond Light Source (Didcot, UK) at 100K using a Pilatus 6M detector. Diffraction data were integrated and scaled using XDS (33) and symmetry related reflections were merged with Aimless (34). The resolution cut off used for structure determination and refinement was determined based on the CC1/2 criterion proposed by Karplus and Diederichs (35) The structure

of S1PL2021 was determined by molecular replacement using a model based on PBD code: 3MAD, modified to match the target sequence using Chainsaw (36). A single solution comprising two molecules in the asymmetric unit was found using Phaser (37). The initial model was rebuilt using Phenix.autobuild (38) followed by cycles of refinement with Phenix.refine (39) in the Phenix programme suite (40) and manual rebuilding in Coot (41) The final model was refined with isotropic B-factors and the model was validated using MolProbity (42) Structural superimpositions were calculated using Coot. Crystallographic figures were generated with PyMOL (43)

RESULTS

Identification of putative *Burkholderia* S1PLs by BLASTp search

BLASTp hits for novel bacterial S1PLs were identified in the genomes of various species of *Burkholderia* by using the 507 amino acid sequence of the confirmed bacterial S1PL from *S. thermophilum, St*S1PL (Uniprot:Q67PY4) as the query sequence (20, 44). Several putative S1PLs with >40 % sequence identity were identified in the known human pathogen *B. pseudomallei* and in *B. thailandensis,* a non-pathogenic model organism (45). Strikingly, all representatives of these species each encode two putative S1PLs, with the two genes located in close proximity within each species. This is exemplified by *B. pseudomallei* strain K96243 which contains two genes in close proximity with locus IDs of *BPSS2021* (S1PL2021) and *BPSS2025* (S1PL2025) that display 86.3 % amino acid sequence identity between them and 43.9 % and 43.1 % identity respectively to the confirmed *St*S1PL (supplementary Fig. S1 and S2). These two predicted S1PLs also contained the conserved residues involved in binding the PLP cofactor (44).

To characterise the recombinant forms of these putative S1PLs we began by expressing S1PL2021 in *E. coli*, but the ORF displayed two potential start codons. The sequence identity between S1PL2021 with *St*S1PL was low at the N-termini (supplementary Fig. S2) with the pairwise alignment beginning at M47 of *St*S1PL. This aligns well with a conserved MDLEEG motif found in S1PL2021 and the other S1PL homologs in *Burkholderia* species and two clones were prepared; one that began at the conserved MDLEEG motif (named S1PL2021) and another that expressed an extended construct (named S1PL2021 (N-EXT)).

Purification and characterisation of S1PL2021 and S1PL2021 N-EXT.

Recombinant S1PL2021 was expressed in *E. coli* from plasmid pET-28a as a hexa-histidine (6His) C-terminal fusion. A standard purification procedure using immobilised nickel affinity (IMAC) and size-exclusion chromatography (SEC) yielded milligram amounts of pure recombinant protein S1PL2021 that was predominantly dimeric in solution (supplementary Fig. S3A and S3B). A similar strategy was used to prepare recombinant S1PL2025 (supplementary Fig. S3C and S3D). Analysis of S1PL2021 suggested that PLP was bound to the protein since the UV-visible spectrum displayed absorbances at ~330 nm and ~420 nm that are characteristic of PLP-dependent enzymes (supplementary Fig. S3E). A similar PLP binding spectrum was

observed with S1PL2025 (supplementary Fig. S3F). In contrast, the alternative construct, S1PL2021 N-EXT purified in an identical manner to the S1PL2021 but failed to display any PLP binding (supplementary Fig. S3G). These results confirmed that these truncated versions of S1PL2021 and S1PL2025 bound PLP and these forms of the protein were used throughout the study.

Substrate and product binding to S1PL2021.

When the substrate S1P (100 µM) was added to the PLP-bound form of S1PL2021 (15 µM) and the resulting mixture analysed by UV-Vis spectroscopy, the peak at 420 nm decreased along with an increase in the 330 nm region over a period of 30 mins suggesting that S1P is binding to S1PL2021 (Fig. 2A). Addition of the product PE (10 mM) to the protein also showed changes in the UV-visible region (maxima at ~320 nm) with an additional blue shift to ~395 nm, although this occurred at a much slower rate than for S1P (Fig. 2B). According to the putative S1PL mechanism proposed by Bourquin *et al* (44) these spectroscopic changes are due to the formation of the PLP-S1P and PLP-PE external aldimine intermediates that are bound to S1PL (supplementary Fig. S4). We carried out similar UV-vis analysis of the binding of S1P and PE to the S1PL2025 enzyme (Fig. 2C and 2D). The changes in the UV-vis spectra were similar when we compare the incubation of S1PL2021 and S1PL2025 with S1P. In contrast, when we compared the spectra from the incubations of the product PE with both enzymes, we did not observe the 420 to 395 nm shift in the S1PL2025 enzyme and the changes took longer to occur compared with the S1PL2021 enzyme. These combined data suggest that, despite having highly similar amino acid sequences (86 %), the two S1PL isoforms display small differences in their cofactor, substrate and product binding that deserves further investigation. We also used UV-vis spectroscopy to show that S1PL2021 could also bind the non-phosphorylated substrate D-*erythro* sphingosine (Fig. 2E). Addition of this substrate led to similar changes in the PLP region of the UV-vis spectrum that were observed for S1P, although this took significantly longer (~4 hours).

Confirmation that S1PL2021 is an S1PL

To determine if the *B. pseudomallei* S1PL2021 and S1PL2025 displayed S1PL activity we used an established mass spectrometry-based method developed by Berdyshev and colleagues that has been used to detect S1PL

activity in mammalian liver microsomes (26). This method relies on extracting the 2E-HEX aldehyde product of the S1PL reaction and forming a stable semicarbazone derivative (2E-HEX SC, $[M+H]^+$ $C_{17}H_{34}N_3O^+$, predicted m/z = 296.3 Da, observed m/z = 296.3 Da) using semicarbazide hydrochloride (Fig. 3A). Recombinant S1PL2021 was incubated with 260 µM S1P and aliquots taken for semicarbazone derivitisation. Additional positive and negative controls were prepared and treated in an identical manner and the results analysed using ESI-MS (Fig. 3B-E). The positive control used previously synthesized 2E-HEX and gave a single peak at 296.3 Da matching the expected semicarbazone derivative (Fig. 3B). This peak was absent in the no enzyme control with the S1P substrate ($[M+H]^+$, predicted $C_{18}H_{39}NO_5P^+$ m/z = 380.2 Da, observed m/z = 380.4 Da, Fig. 3C). The reaction catalysed by S1PL2021 resulted in a signal with m/z = 296.3 Da indicating the production of the 2E-HEX SC species and confirming S1PL2021 displayed S1PL activity (Fig. 3D). In contrast, the no substrate control lacked both the above peaks (Fig. 3E).

FALDH coupled assay suitability/optimisation

The ESI-MS method confirmed that S1PL2021 displays S1PL activity, therefore we went on to develop a convenient continuous spectroscopic assay in order to perform steady-state kinetic analysis of S1PL. We took advantage of the activity of fatty aldehyde dehydrogenase (FALDH), the next enzyme in the SL metabolic pathway (Fig. 1). The human FALDH (also known as ALDH3A2) has been cloned and recombinant enzyme has been isolated from *E. coli* by Lloyd *et al.* (46) so this presented an attractive candidate for the development of a coupled assay. A commercially available cDNA clone (Source BioScience, product code IRAUp969B0810D in plasmid pOTB7) was used to construct an expression clone of the full length FALDH protein (isoform 1), however, in our hands, this initial construct was insoluble (data not shown). A sequence alignment between human FALDH and rat ALDH3A1, which lacks a hydrophobic C-terminal transmembrane region, guided the preparation of a second, truncated clone (supplementary Fig. S5). This shorter variant expressed well in *E. coli* and we were able to isolate mg quantities of recombinant His-tagged human FALDH (supplementary Fig. S6). By monitoring aldehyde substrate-dependent, NADH formation at 340 nm we established that the fully saturated substrates, hexadecanal and tetradecanal and, most importantly, the unsaturated 2E-HEX, were substrates for this recombinant FALDH (Fig. 4A). Using varying 2E-HEX substrate concentrations (0-260 µM) the reaction was linear over the first 3 minutes and the limit of detection was

determined to be ~4 µM 2E-HEX (supplementary Fig. S7A). We performed Michaelis Menten analysis and determined the kinetic values for 2E-HEX with a K_M = 19.4 ± 3.2 µM and k_{cat} = 0.22 ± 0.01 s^{-1} recorded. (Fig. 4B, Table 1). The active FALDH was then coupled to both S1PL2021 and S1PL2025 in the presence of S1P and NAD^+ at 30°C to determine the kinetic constants of both S1PL enzymes. The initial reaction rates were linear over a S1P concentration range of 0-175 µM. Therefore S1PL activity could be quantified in a continuous fashion (down to a S1P substrate concentration of ~10µM) (supplementary Fig. S7B and S7C) and allowed the determination of the kinetic constants of both *B. pseudomallei* S1PLs. The values for each are as follows; S1PL2021 (K_M = 48.2 ± 9.4 µM and k_{cat} = 0.015 ± 0.003 s^{-1}) and S1PL2025 (K_M = 50.2 ± 8.3 µM and k_{cat} = 0.008 ± 0.0005 s^{-1}) (Fig. 4C and 4D, Table 1). Thus this new assay offered a convenient way of measuring the activity of recombinant S1PL. Based on the S1PL sequence alignment residue K271 of S1PL2021 is predicted to bind the essential PLP cofactor (supplementary Fig. S2). A S1PL2021 K271A mutant was prepared and when used in the coupled assay this variant was essentially inactive in comparison to the wild type enzyme (Fig. 4E). We also used the assay to determine if S1PL2021 used *D-erythro* sphingosine as a substrate and found that it displayed ~8% activity compared with S1P (Fig. 4F).

Structural characterisation of S1PL2021

The further characterise the *Burkholderia pseudomallei* S1PL enzymes we subjected S1PL2021 to crystallisation trials using commercially available screens. Crystals with a monoclinic morphology were grown in 20 % (v/v) PEG400, 10 % (v/v) 1-propanol. Diffraction data on cryocooled crystals were collected on a single crystal at Diamond Light Source (beamline I03) to a maximum resolution of 2.1 Å in space group P1 2_1 1. The structure of S1PL2021 was determined by molecular replacement using a monomer of the *S. thermophilum* S1PL structure as the template (PDBID: 3MAD). The final refined model contains a dimer of S1PL with the PLP cofactor present as an internal aldimine with residue K271 in each chain (Fig. 5A). There was no clear electron density present for residues before L10; between residues H430 and A455; and for the His6 tag after residue P472 at the C-terminus; residues in these regions were omitted from the final model.

The S1PL2021 structure conformed to the typical type I PLP dependent fold seen in the group II decarboxylase subfamily (11, 44). The overall architecture of the protein closely matches homologous structures, with excellent

overall alignment of S1PL2021 with published structures (supplementary Fig. S8A, supplementary Table S1). The structure has an N-terminal domain (residues 10-55), which is primarily involved in dimerization; a large cofactor-binding central domain (residues 56-320); a short C-terminal domain (residues 321 – 430); and a C-terminal extension (431 – 471) (Fig. 5A). The latter domain is partially disordered, with the region between residues 431 and 455 not visible in the experimental electron density; this region sits close to the cofactor and substrate-binding region and may change conformation on ligand binding.

The cofactor-binding site at the dimer interface shows excellent electron density for the PLP cofactor, which was found to bind to K271 via a Schiff base as an internal aldimine (Fig. 5B). Coupled with the high conservation of active site residues with other members of the S1PL family across bacteria, yeast and human (supplementary Fig. S8B, supplementary table S2), our structural data confirm the assignment of S1PL2021 as a member of the sphingosine-1-phosphate lyase family (EC number 4.1.2.27) and given the high sequence identity of S1PL2025 (86 %) suggest that this is also a S1PL family enzyme. The cluster of residues involved in PLP binding are highly conserved across the members of the S1PL family, with these residues adopting the same orientation in published crystal structures (supplementary Fig. S8B). Analysis of the active site shows that the pyridine ring is held in place between C235 and H159 with π-stacking interactions to the latter residue; the nitrogen of the pyridine group forms a hydrogen bond to D233 (fig. 5B). The PLP phosphate group forms hydrogen bonds with the sidechain of H270 and the backbone nitrogens of G126, T127, and S313 from the partner chain. The K271 chain is held in place through a hydrogen bond between D268 and the sidechain nitrogen that forms the Schiff base with PLP.

The dimer observed in the crystal structure of S1PL2021 is the native form of this protein (Fig. 5A), as the cofactor-binding site and ligand-binding funnel is formed between the two monomers (supplementary Fig. S9A and S9B). The dimerization interface buries nearly 50 % of the total surface area of each monomer with a total buried area of 6430 $Å^2$; the interface is stabilised by 52 hydrogen bonds and 32 salt bridges. The observation that S1PL2021 is unable to bind PLP when expressed in the full-length form as annotated in the genome is explained by the fact that any significant extension of the N-terminus of the structure from that seen in the crystal structure would potentially occlude the substrate binding funnel and PLP binding site (supplementary Fig. S9A). The substrate-binding funnel of S1PL2021 is formed between the two monomers, with one monomer providing a primarily positively charged surface and the other a negatively charged surface (supplementary Fig.

S9B). The missing region of the protein that forms the C-terminal extension is likely to play a role in substrate recognition given its position over the funnel and its inherent flexibility in this structure.

DISCUSSION

Sphingolipids and ceramides have been shown to be important players in various eukaryotic cell functions. The amino alcohol core structure of all SLs is built from L-serine and a long chain fatty acid and further elaborated by a series of enzymes that increase their complexity by phosphorylation, oxidation and acylation (1). Cells maintain a balance of SLs and ceramides via highly regulated synthetic and metabolic pathways whose control mechanisms are still not fully understood. Perturbation of this balance has now been linked to a number of diseases such as cancer, atherosclerosis, autoimmunity and infection (5, 6). A key regulatory mechanism involves the breakdown of the potent signalling molecule S1P by S1PL and *S. cerevisiae* has been a useful model organism where the pathways for de novo biosynthesis, recycling and degradation of SLs have been delineated (47). Indeed, the first S1PL gene (*dpl1*) was characterised in *S. cerevisiae* by Saba and colleagues and they showed that a Dpl1 mutant strain was not only highly sensitive to exogenous sphingosine but also accumulated intracellular S1P upon exposure to sphingosine (9). In contrast to higher order organisms, relatively few studies have been carried out to investigate the role of SLs biosynthesis and metabolism in bacterial species. Of these, it is interesting to note that microbes from the human microbiome – *P. gingivalis* from the oral cavity and the gut commensal *Bacteroides fragilis* make SLs with unusual structural features (14–16). Their roles in bacterial metabolism, as well as their interaction within the host environment, are currently under investigation (48) .

Burkholderia are a group of interesting bacterial species that can cause life-threatening infections and have a reputation as being highly resistant to antibiotics (49–51) They appear to lack the ability to synthesise *de novo* SLs since analysis of their genomes suggest that the biosynthetic genes are absent. We were therefore interested to discover that *B. pseudomallei* K96243 encodes two highly homologous ORFs that display moderate (~40%) sequence identity to the *S. thermophilum* S1PL query sequence (supplementary Fig. S1 and S2). The two ORFs, BPSS2021 and BPSS2025 (annotated as decarboxylases in the genome) also display 86 % sequence identity to each other. Since a more detailed sequence and structural analysis revealed that both ORFs contained conserved residues important for binding the PLP cofactor and enzyme catalysis we hypothesised that these genes encode S1PLs. Therefore, we cloned, expressed and purified recombinant forms of both S1PLs and UV-vis analysis showed that they bound the PLP cofactor (supplementary Fig. S3). Monitoring the changes in the UV-vis spectrum of PLP-dependent enzymes can be a useful tool to study how substrates, products and

inhibitors interact with these enzymes. The PLP binding region of holo-S1PL2021 showed changes upon addition of 100 µM S1P with an initial sharp rise in the 330 nm region, followed by a slower increase at this wavelength (Fig. 2A). At the same time there was a decrease in the absorbance at 420 nm. Addition of the product PE to S1PL2021 led to the appearance of a peak at 320 nm and a decrease at 420 nm with a shift to 395 nm (Fig. 2B). We carried out the same substrate and product binding analyses with S1PL2025 (Fig. 2C and 2D) and the general trend was similar, unsurprising as they are 86% identical. In contrast, in their studies with the *S. thermophilum* S1PL, Bourquin and colleagues observed the transient appearance of two peaks (403 nm and 420 nm) which they tentatively assigned as the PLP-S1P and PLP-PE external aldimines in the putative S1PL reaction mechanism (intermediates 3 and 7 respectively in supplementary Fig. 4). These peaks appeared immediately upon S1P addition, and then reduced over 5 minutes until the spectrum resembled that of the starting PLP-bound, holo- form of the enzyme. Moreover, they noted that the yeast S1PL UV-vis spectrum did not show any changes upon S1P addition and they concluded that this enzyme was inactive. Our mass spectrometry and FALDH coupled assay (described below) prove both *Burkholderia* S1PL2021 and S1PL2025 are active. Given that the S1PLs did not regenerate the holo- form spectrum, it suggests differences between the *Burkholderia* S1PLs and the *S. thermophilum* S1PL with which they share ~40% sequence identity. Our results could indicate the slow release of products (PE or 2E-HEX) or the build up of a hitherto uncharacterised intermediate.

The ability to measure S1PL activity using a convenient method would help expand structural and mechanistic studies of the enzyme in all organisms. Since the first discovery of S1PL activity in mammalian cells by Stoffel and colleagues, (52) who used a ^{14}C-labelled substrate, a number of S1PL assays have been developed that use radioactive, fluorescent and fluorogenic substrates and substrate analogues. One of the earliest methods used incorporation of ^{3}H labels into the S1P substrate and thin layer chromatography (TLC) and liquid scintillation counting (LSC) analysis of the products. This was applied to the study of the S1PL enzyme in rat liver and values of K_M = 9 µM and V_{max} = 0.082 pmol/min/µg were determined (22). Bandhuvula and colleagues synthesized a fluorescent, NBD-labelled S1P homolog (S1P-C18NBD) that was used to analyse the human S1PL in HEK293 cells and gave values of K_M = 14.6 µM and V_{max} = 3.4 x 10^{-4} pmol/min/µg (23). These authors then prepared a more stable fluorescent S1P-C14 Bodipy analogue that was used to analyse the human enzyme again in HEK293 cells that gave values (K_M = 35 µM, V_{max} = 5.1 x 10^{-4} pmol/min/µg) in good

agreement with the previous study (24). An alternative, clever strategy retained the phosphorylated amino alcohol structure of the natural S1P substrate and combined it with an ether-linked, coumarin-based reporter to generate a substrate that, upon S1PL-catalysed cleavage, breaks down by β-elimination to a highly-fluorescent umbelliferone product. Although highly sensitive, this non-native substrate displays a high K_M (152 μM) for the S1PL in mouse embryonic fibroblasts (MEFs) and the fluorescence was significantly reduced in the presence of Triton-X100 that is used to solubilise the S1P (25). Mass spectrometry (MS)-based techniques have also been developed that involve the derivitization of the 2E-HEX aldehyde product with reagents (usually hydrazides) that improve ionization efficiency. The first MS-based method was developed by Berdyshev and colleagues to characterise the S1PL activity in mouse liver microsomal extracts (K_M = 5.7 μM, V_{max} = 0.171 pmol/min/μg) (26). A similar gas chromatography/electron ionisation (GC/EI) MS method used pentafluorobenzoyloxime derivitization of the 2E-HEX to analyse the S1PL in MEFs (K_M = 6 μM, V_{max} = 0.374 pmol/min/μg) (27). Novartis have recently identified the human S1PL as an attractive target for the development of therapeutics and developed a high throughput, MS-based method to screen for novel inhibitors (11). By using nicotinylhydrazide (Isoniazid) modification of the 2E-HEX they obtained the first data on purified, recombinant human S1PL (K_M = 5.2 ± 0.9 μM). Most recently, Suh and colleagues developed a stable isotope dilution method using an internal D-labelled standard to also determine the values for recombinant human S1PL in good agreement with the value determined by Novartis (K_M = 4.67 μM, V_{max} = 2.6 pmol/min/μg) (53).

We decided to use an MS-based method to confirm that the recombinant *B. pseudomallei* S1PL2021 isoform catalysed the degradation of S1P to 2E-HEX (Fig. 3). Since this end-point method involves a number of liquid handling steps (derivitization, organic extraction) and requires an internal standard, we sought to develop a convenient, continuous spectroscopic assay that could be used for S1PL analysis. Our choice of coupling enzyme was informed by our knowledge of the SL degradative pathway (Fig. 1). In mammals, the 2E-HEX aldehyde product of the S1PL enzyme is oxidised to the acid by a fatty aldehyde dehydrogenase (FALDH, also known as ALDH3A2, UniProt Code: P51648) in an NAD^+-dependent manner that can be monitored at 340 nm. Human FALDH has been the subject of various studies since it has been linked to the SL-metabolic disease Sjögren–Larsson syndrome (8). Previously, recombinant, full-length human FALDH had been isolated by Lloyd *et al* who showed that extraction of the enzyme from *E. coli* required the use of the anionic detergent N-lauroylsarcosine (46). This enzyme displays broad substrate specificity and could use saturated fatty aldehydes

of varying chain lengths (from C5 to C18) with K_M values in the low µM range (4-35 µM) and k_{cat} values (~1 s^{-1}) that would deem it suitable as a coupling enzyme. We prepared recombinant, N-terminally His-tagged human FALDH by relatively straightforward, soluble expression in *E. coli* once we had removed the C-terminal 36 residues that contained a predicted potential transmembrane (TM) domain (supplementary Fig. S5). Of note, Lloyd *et al* did not prepare 2E-HEX but did show that the FALDH used the commercially available, unsaturated *cis*-11-hexadecenal as a substrate. We found that our truncated, recombinant FALDH was not only active with the saturated C14 and C16 fatty aldehydes but, more importantly, also used the synthetic 2E-HEX as a substrate and we determined kinetic values (K_M = 19.4 ± 3.2 µM and k_{cat} = 0.22 ± 0.01 s^{-1}) that suggested that it would make a suitable coupling partner for the determination of S1PL activity (Fig. 4A and B).

During our work a detailed x-ray structure and mechanistic study of the human FALDH was published with a view to understanding the substrate specificity of the enzyme and the impact of mutations that cause SLS (54). In this paper the FALDH construct contained an N-terminal streptavidin affinity tag and, in comparison to our truncation, only removed the C-terminal 22 amino acids, the minimum based on the proposed TM region. This construct was catalytically active with C8, C12 and C16 saturated aldehyde substrates in the presence of 0.1% Triton X100 but they noted that removal of a 40 amino acid section resulted in a drastic reduction in activity with the longer acyl-chain length substrates. The x-ray structure of the FALDH (PDB: 4QGK, 2.1 Å resolution) revealed that, as well as being involved in the TM interaction, the C-terminal domain also contained a gatekeeper helix that is proposed to be involved in substrate specificity (supplementary Fig. 5B). This structure allowed us to rationalise how our truncation of the C-terminal hydrophobic element increased the solubility of our FALDH construct whilst retaining enough of the helix to maintain good activity towards long acyl chain substrates, crucially including 2E-HEX (supplementary Fig. S5A and S5B). We combined our FALDH with the purified *Burkholderia* S1PL2021 and S1PL2025 enzymes in the presence of PLP, NAD^+ and S1P solubilised in Triton X100. We observed that the assay was linear over a practical substrate range (0-175 µM) and determined kinetic values for S1PL2021 (K_M = 48.2 ± 9.4 µM and k_{cat} = 0.015 ± 0.003 s^{-1}) and S1PL2025 (K_M = 50.2 ± 8.3 µM and k_{cat} = 0.008 ± 0.0005 s^{-1}) (Fig. 4C and Fig. 4D, Table 1). Since both isoforms display such high sequence identity it is not surprising that they display similar K_M values for S1P, however we noted that the S1PL2025 was 50% slower than the S1PL2021 isoform. Although we used this assay to only study the Burkholderia S1PLs, we think that this convenient FALDH-coupled method will be of use to those working with S1PLs from other

organisms (e.g. yeast and human). It will be interesting to determine if it can also be applied not only to purified recombinant enzymes and HTP S1PL inhibitor screens, but also whole cell lysates.

To explore the structures of these novel *Burkholderia* S1PLs we used our optimised expression system for S1PL2021 to prepare crystals that diffracted to 2.1 Å. Using the *S. thermophilum* S1PL structure (PDB: 3MAD) as a template for molecular replacement the structure refined well and the enzyme displayed the canonical Type I fold of the PLP superfamily of enzymes (Fig. 5A, suppl. Fig. 8A) (55). Furthermore, it belongs to the group II decarboxylase subfamily which is typical of S1PLs from other species. The monomer has a three domain architecture, a short N-terminal domain, a large central domain that binds the well resolved PLP cofactor bound as an internal aldimine/Schiff base to K271, and an extended C-terminal domain (Fig. 5A). As well as K271, comparison with other S1PLs identifies conserved residues involved in PLP binding; C235 and H159 binds to the pyridine ring, residues G126, T127, H270, S313* (from the other subunit) coordinate the phosphate group and D233 is involved in salt bridge formation of the pyridine nitrogen (Fig. 5B, supplementary table S2). An overlay of all the well-refined structures of S1PLs in the PDB with PLP and/or Pi bound shows that the S1PL2021 active site architecture is well conserved (Suppl. Fig. 8B, supplementary table S2). Given its role in anchoring the PLP cofactor it is not surprising that mutation of the conserved K271 drastically reduces S1PL activity to 2% when compared to wild type (Fig. 4E). Both S1PLs showed activity with S1P as a substrate but we also wished to explore if the phosphate of S1P was required for activity. Since we had observed binding of D-*erythro* sphingosine to S1PL2021 (Fig. 2E) by UV-vis spectroscopy, it was interesting to find that this isoform did catalyse breakdown of this non-phosphorylated sphingolipid (~8% activity compared to S1P, Fig. 4F). Thus it appears that the Burkholderia S1PLs display some substrate promiscuity and may be able to break down a range of both phosphorylated and non-phosphorylated sphingolipids. In future it will be interesting to carry out a comprehensive substrate analysis with these enzymes and explore their specificity with respect to acyl chain length, C1 head group, the oxidation state at C4-C5 (sphingosine/sphinganine) and the C2-C3 stereochemistry (*erythro*/*threo*).

Although the crystal structures of S1PLs from *S. thermophilum*, *S. cerevisiae*, human and *L. pneumophila* have been solved the exact nature of substrate binding and enzyme catalysis are still unclear since the structure of a S1P-bound complex has not been determined (44, 56, 57). For example, in the putative mechanism, the active site base that deprotonates the S1P hydroxyl leading to the retro-aldol like cleavage of

the substrate has not been identified (supplementary Fig. S4). Bourquin *et al* described a *S. thermophilum* S1PL:PLP-PE product complex as well as a S1PL:PLP internal aldimine with a phosphate ion bound and together these structures hinted at the residues involved in binding the phosphate of S1P. Despite screening numerous conditions we were unable to trap the wild type S1PL2021:PLP-S1P external aldimine complex since we assume the enzyme catalyses the rapid break down of the S1P. We recently used mutagenesis of an active site lysine that allowed us to capture the PLP-dependent enzyme serine palmitoyl transferase (SPT) bound to the inhibitor myriocin (58). We used a similar strategy to screen crystals of the S1PL2021 K271A mutant for S1P binding but this has so far failed to yield a structure (data not shown). To date the exact residues involved in binding the S1P acyl chain are still not known but an overlay of all available S1PLs suggests the presence of hydrophobic funnel on the surface which leads down into the active site (supplementary Fig. S9). It is interesting that one of the differences between the two enzymes is at position 401; this is a histidine in S1PL2021 and glutamine in S1P2025. This change could contribute to the 50% difference in activity between the two isoforms. In future, swapping the histidine at position 401 for glutamine (and vice versa) between the two forms, as well as mutating other potential residues should identify those involved in substrate binding and catalysis. Our continuous S1P assay will be useful for screening the activity of these and any other mutants.

Since human S1PL has recently been identified as an attractive target for drug discovery, both Novartis and AbbVie have undertaken medicinal chemistry programmes to identify potent inhibitors (56, 59). The determination of the structures of human S1PL and of the "humanised" *S. thermophilum* S1PL in complex with various inhibitors (PDB codes : (PDB codes: 4Q6R, 5EUE and 5EUD respectively) have highlighted how these molecules block the substrate-binding funnel. It will also be interesting to test these and other S1PL inhibitors against various bacterial S1PLs with a view to screen them for antibacterial activity.

To our knowledge, this is the first time that two highly-related S1PLs have been identified in the same organism. At present, this phenomenon appears to be exclusive to species within the *Burkholderia* genus. The *Burkholderia* genus encompasses a remarkably diverse and versatile group of bacteria including environmentally-beneficial species as well as pathogens of animals, humans and plants. It is notable that our search of available genomes identified that *Burkholderia*-encoded S1PLs are restricted to *B. pseudomallei* and *B. thailandensis*, both of which are facultative intracellular species. This is consistent with the bacterial S1PLs contributing to pathogenesis during infection of host cells, as has recently been described for *Legionella*-

encoded S1PL (57). The ability to invade, survive and replicate within host cells is central to the pathogenesis of *B. pseudomallei* (60) and whilst *B. thailandensis* is a highly attenuated relative to *B. pseudomallei*, it displays a similar intracellular phenotype (61) and as such is a valuable model organism for studying the intracellular lifestyle of *B. pseudomallei*. SLs have been shown to be key players in cell homeostasis during stress such as that caused by bacterial infection (62). They mediate crosstalk between apoptosis and autophagy, the two major mechanisms of controlled cell death (63). Recently, studies on *L. pneumophila*, the causative agent of Legionnaires' disease, have sought to understand the role that the *L. pneumophila* S1PL plays in its ability to survive intracellularly (57). It was found that *L. pneumophila* S1PL activity alone prevented an increase in sphingosine levels in infected host cells and this led to an inhibition of autophagy during macrophage infection. This work revealed the disruption of host SL biosynthesis as a novel mechanism used by intracellular pathogens to inhibit autophagy.

Since Burkholderia appear to not produce sphingolipids such as S1P, the identity of the "true" intracellular substrate(s) for these enzyme is the subject of conjecture. We have shown that S1PL2021 can also degrade sphingosine as well as S1P, and it will be interesting to study a comprehensive range of potential substrates with each S1PL isoform to define their specificity. Burkholderia would most likely encounter high concentrations of S1P only during infection of a mammalian host and this would require the S1PLs to be secreted. In a recent complementary study we have discovered that the two S1PL homologs present in *B. thailandensis* (BTH_II0309 and BTH_II0311, Fig. S1) are found in the extracellular supernatant in a pH-dependent manner (Custodio et al, Mol Microbiol. 2016 Sep 15. doi: 10.1111/mmi.13531). We are currently investigating whether both these S1PLs form part of a higher order complex as pairs of homo- or hetero- dimers but initial native gel electrophoresis suggests the presence of larger complexes. We also found that when expressed alone, BTH_II0309 and BTH_II0311 could each partially restore resistance to 10 μM sphingosine treatment of a yeast Dpl1 mutant and full resistance was displayed by cells expressing both S1PLs. Our future work will determine whether the *B. pseudomallei* S1PL2021 and S1PL2025 can also complement the yeast Dpl1 mutant and are secreted in a similar way to the *B. thailandensis* isoforms. We studied the functional roles of the Burkholderia S1PLs and found they were required for virulence in a Galleria wax moth larvae model and survival in murine macrophages (Custodio et al.). Of particular relevance to the current study, we discovered that a *B. pseudomallei* S1PL2025 mutant displayed a much reduced virulence phenotype (80% survival)

compared to the wild type organism (100% mortality) using a murine infection model in BALB/c mice. We are currently constructing the *B. pseudomallei* S1PL2021 knock out and a double mutant to study their virulence phenotypes. In summary, our work has characterised two S1PL homologs in *B. pseudomallei* and, when combined with recent studies on the emerging roles of bacterial S1PLs in pathogenesis, suggests that these enzymes merit further study.

Acknowledgements

The authors thanks the following for funding: The Biotechnology and Biological Sciences Research Council (BBSRC) for an EastBio Doctoral Training Programme PhD studentship award to C McLean (BB/J01446X/1) and a grant awarded to DJ Campopiano (BB/I013687/1) that supported J Lowther and DJ Clarke. R Custodio was supported by the Defence Science and Technology Laboratory under contract DSTLX-1000060221 (WP1). We thank the staff of the Diamond Light Source, UK for help with data collection. The authors thank Prof. John RW Govan (University of Edinburgh) for his suggestions regarding *Burkholderia* strains and enthusiastic support of this work. We also thanks Dr. Kevin Ralston for help in the synthesis of 2E-HEX. The data associated with this paper is available to download (http://dx.doi.org/10.7488/ds/1412).

References

1. Merrill, A. H.. 2011. Sphingolipid and glycosphingolipid metabolic pathways in the era of sphingolipidomics. *Chem. Rev.* **111**: 6387–6422.

2. Lingwood, D., and K. Simons. 2010. Lipid rafts as a membrane-organizing principle. *Science*. **327**: 46–50.

3. Fyrst, H., and J. D. Saba. 2010. An update on sphingosine-1-phosphate and other sphingolipid mediators. *Nat. Chem. Biol.* **6**: 489–497.

4. Pyne, S., and N. J. Pyne. 2000. Sphingosine 1-phosphate signalling in mammalian cells. *Biochem. J.* **349**: 385–402.

5. Yester, J. W., E. Tizazu, K. B. Harikumar, and T. Kordula. 2011. Extracellular and intracellular sphingosine-1-phosphate in cancer. *Cancer Metastasis Rev.* **30**: 577–597.

6. Spiegel, S., and S. Milstien. 2003. Sphingosine-1-phosphate: an enigmatic signalling lipid. *Nat. Rev. Mol. Cell Biol.* **4**: 397–407.

7. Cuvillier, O., G. Pirianov, B. Kleuser, P. G. Vanek, O. A. Coso, S. Gutkind, and S. Spiegel. 1996. Suppression of Ceramide-Mediated Programmed Cell Death by Sphingosine-1-Phosphate. *Nature*. **381**: 800–803.

8. Nakahara, K., A. Ohkuni, T. Kitamura, K. Abe, T. Naganuma, Y. Ohno, R. A. Zoeller, and A. Kihara. 2012. The Sjrogren-Larsson Syndrome Gene Encodes a Hexadecenal Dehydrogenase of the Sphingosine 1-Phosphate Degradation Pathway. *Mol. Cell*. **46**: 461–471.

9. Saba, J. D., F. Nara, A. Bielawska, S. Garrett, and Y. A. Hannun. 1997. Communications : The BST1 Gene of *Saccharomyces cerevisiae* Is the sphingosine 1-phosphate lyase. 26087–26090.

10. Van Veldhoven, P. P., S. Gijsbers, G. P. Mannaerts, J. R. Vermeesch, and V. Brys. 2000. Human sphingosine-1-phosphate lyase: cDNA cloning, functional expression studies and mapping to chromosome 10q22(1). *Biochim. Biophys. Acta*. **1487**: 128–134.

11. Weiler, S., N. Braendlin, C. Beerli, C. Bergsdorf, A. Schubart, H. Srinivas, B. Oberhauser, and A. Billich. 2014. Orally Active 7-Substituted (4-Benzylphthalazin-1-yl)-2- methylpiperazin-1-yl]nicotinonitriles as Active-Site Inhibitors of Sphingosine 1-Phosphate Lyase for the Treatment of Multiple Sclerosis. *J. Med. Chem.* **57**: 5074–5084.

12. Martinez, M., and A. Ovalle. 2013. *Sphingomonas paucimobilis*. *Rev. Chil. Infectol.* **30**: 107–110.

13. Keck, M., N. Gisch, H. Moll, F. J. Vorhölter, K. Gerth, U. Kahmann, M. Lissel, B. Lindner, K. Niehaus, and O. Holst. 2011. Unusual outer membrane lipid composition of the gram-negative, lipopolysaccharide-lacking myxobacterium *Sorangium cellulosum* So ce56. *J. Biol. Chem.* **286**: 12850–12859.

14. Wieland Brown, L. C., C. Penaranda, P. C. Kashyap, B. B. Williams, J. Clardy, M. Kronenberg, J. L. Sonnenburg, L. E. Comstock, J. A. Bluestone, and M. A. Fischbach. 2013. Production of α-Galactosylceramide by a Prominent Member of the Human Gut Microbiota. *PLoS Biol.* **11**. e1001610.

15. An, D., C. Na, J. Bielawski, Y. a Hannun, and D. L. Kasper. 2011. Membrane sphingolipids as essential molecular signals for Bacteroides survival in the intestine. *Proc. Natl. Acad. Sci. U. S. A.* **108 Suppl** : 4666–4671.

16. Mun, J., A. Onorato, F. C. Nichols, M. D. Morton, A. I. Saleh, M. Welzel, and M. B. Smith. 2007. Structural confirmation of the dihydrosphinganine and fatty acid constituents of the dental pathogen *Porphyromonas gingivalis*. *Org. Biomol. Chem.* **5**: 3826–3833.

17. Degtyar, E., T. Zusman, M. Ehrlich, and G. Segal. 2009. A Legionella effector acquired from protozoa is involved in sphingolipids metabolism and is targeted to the host cell mitochondria. *Cell. Microbiol.* **11**: 1219–1235.

18. Rolando, M., P. Escoll, T. Nora, J. Botti, V. Boitez, C. Bedia, C. Daniels, G. Abraham, P. J. Stogios, T. Skarina, C. Christophe, D. Dervins-Ravault, C. Cazalet, H. Hilbi, T. W. T. Rupasinghe, D. Tull, M. J. McConville, S. Y. Ong, E. L. Hartland, P. Codogno, T. Levade, T. Naderer, A. Savchenko, and C. Buchrieser. 2016. *Legionella pneumophila* S1P-lyase targets host sphingolipid metabolism and restrains autophagy. *Proc. Natl. Acad. Sci.* **113**: 1901-1906.

19. White, N. J. 2003. Melioidosis. *Lancet*. **361**: 1715–1722.

20. Winsor, G. L., B. Khaira, T. Van Rossum, R. Lo, M. D. Whiteside, and F. S. L. Brinkman. 2008. The Burkholderia Genome Database: Facilitating flexible queries and comparative analyses. *Bioinformatics*. **24**: 2803–2804.

21. Holden, M. T. G., R. W. Titball, S. J. Peacock, A. M. Cerdeño-Tárraga, T. Atkins, L. C. Crossman, T. Pitt, C. Churcher, K. Mungall, S. D. Bentley, M. Sebaihia, N. R. Thomson, N. Bason, I. R. Beacham, K. Brooks, K. A. Brown, N. F. Brown, G. L. Challis, I. Cherevach, T. Chillingworth, A. Cronin, B. Crossett, P. Davis, D. DeShazer, T. Feltwell, A. Fraser, Z. Hance, H. Hauser, S. Holroyd, K. Jagels, K. E. Keith, M. Maddison, S. Moule, C. Price, M. A. Quail, E. Rabbinowitsch, K. Rutherford, M. Sanders, M. Simmonds, S. Songsivilai, K. Stevens, S. Tumapa, M. Vesaratchavest, S. Whitehead, C. Yeats, B. G. Barrell, P. C. F. Oyston, and J. Parkhill. 2004. Genomic plasticity of the causative agent of melioidosis, *Burkholderia pseudomallei*. *Proc. Natl. Acad. Sci. U. S. A.* **101**: 14240–14245.

22. Van Veldhoven, P. P., and G. P. Mannaerts. 1991. Subcellular localization and membrane topology of sphingosine-1-phosphate lyase in rat liver. *J. Biol. Chem.* **266**: 12502–12507.

23. Bandhuvula, P., H. Fyrst, and J. D. Saba. 2007. A rapid fluorescence assay for sphingosine-1-phosphate lyase enzyme activity. *J. Lipid Res.* **48**: 2769–2778.

24. Bandhuvula, P., Z. Li, R. Bittman, and J. D. Saba. 2009. Sphingosine 1-phosphate lyase enzyme assay using a BODIPY-labeled substrate. *Biochem. Biophys. Res. Commun.* **380**: 366–370.

25. Bedia, C., L. Camacho, J. Casas, J. L. Abad, A. Delgado, P. P. Van Veldhoven, and G. Fabriàs. 2009. Synthesis of a fluorogenic analogue of sphingosine-1-phosphate and its use to determine sphingosine-1-phosphate lyase activity. *Chembiochem.* **10**: 820–822.

26. Berdyshev, E. V, J. Goya, I. Gorshkova, G. D. Prestwich, H.-S. Byun, R. Bittman, and V. Natarajan. 2011. Characterization of sphingosine-1-phosphate lyase activity by electrospray ionization-liquid chromatography/tandem mass spectrometry quantitation of (2E)-hexadecenal. *Anal. Biochem.* **408**: 12–18.

27. Reina, E., L. Camacho, J. Casas, P. P. Van Veldhoven, and G. Fabrias. 2012. Determination of sphingosine-1-phosphate lyase activity by gas chromatography coupled to electron impact mass spectrometry. *Chem. Phys. Lipids*. **165**: 225–231.

28. Lüth, A., C. Neuber, and B. Kleuser. 2012. Novel methods for the quantification of (2E)-hexadecenal by liquid chromatography with detection by either ESI QTOF tandem mass spectrometry or fluorescence measurement. *Anal. Chim. Acta*. **722**: 70–79.

29. Liu, Z., Y. Gong, H. Byun, and R. Bittman. 2010. An improved two-step synthetic route to primary allylic alcohols from aldehydes. *New J. Chem.* **34**: 470–475.

30. Chenna, R.. 2003. Multiple sequence alignment with the Clustal series of programs. *Nucleic Acids Res.* **31**: 3497–3500.

31. Kelley, L. A., and M. J. E. Sternberg. 2009. Protein structure prediction on the Web: a case study using the Phyre server. *Nat. Protoc.* **4**: 363–371.

32. Liu, H., and J. H. Naismith. 2008. An efficient one-step site-directed deletion, insertion, single and multiple-site plasmid mutagenesis protocol. *BMC Biotechnol.* **8**: 91.

33. Kabsch, W.. 2010. Xds. *Acta Crystallogr. Sect. D Biol. Crystallogr.* **66**: 125–132.

34. Evans, P. R.. 2011. An introduction to data reduction: Space-group determination, scaling and intensity statistics. *Acta Crystallogr. Sect. D Biol. Crystallogr.* **67**: 282–292.

35. Karplus, A. P. and K. Diederichs. 2012. Linking Crystallographic Model and Data Quality. *Science* **336:** 1030–1033.

36. Stein, N.. 2008. CHAINSAW: A program for mutating pdb files used as templates in molecular replacement. *J. Appl. Crystallogr.* **41**: 641–643.

37. McCoy, A. J., R. W. Grosse-Kunstleve, P. D. Adams, M. D. Winn, L. C. Storoni, and R. J. Read. 2007. Phaser crystallographic software. *J. Appl. Crystallogr.* **40**: 658–674.

38. Terwilliger, T. C., R. W. Grosse-Kunstleve, P. V. Afonine, N. W. Moriarty, P. H. Zwart, L. W. Hung, R. J. Read, and P. D. Adams. 2007. Iterative model building, structure refinement and density modification with the PHENIX AutoBuild wizard. *Acta Crystallogr. Sect. D Biol. Crystallogr.* **64**: 61–69.

39. Afonine, P. V., R. W. Grosse-Kunstleve, N. Echols, J. J. Headd, N. W. Moriarty, M. Mustyakimov, T. C. Terwilliger, A. Urzhumtsev, P. H. Zwart, and P. D. Adams. 2012. Towards automated crystallographic structure refinement with phenix.refine. *Acta Crystallogr. Sect. D Biol. Crystallogr.* **68**: 352–367.

40. Adams, P. D., P. V. Afonine, G. Bunkóczi, V. B. Chen, I. W. Davis, N. Echols, J. J. Headd, L. W. Hung, G. J. Kapral, R. W. Grosse-Kunstleve, A. J. McCoy, N. W. Moriarty, R. Oeffner, R. J. Read, D. C. Richardson, J. S. Richardson, T. C. Terwilliger, and P. H. Zwart. 2010. PHENIX: A comprehensive Python-based system for macromolecular structure solution. *Acta Crystallogr. Sect. D Biol. Crystallogr.* **66**: 213–221.

41. Emsley, P., B. Lohkamp, W. G. Scott, and K. Cowtan. 2010. Features and development of Coot. *Acta Crystallogr. Sect. D Biol. Crystallogr.* **66**: 486–501.

42. Chen, V. B., W. B. Arendall, J. J. Headd, D. A. Keedy, R. M. Immormino, G. J. Kapral, L. W. Murray, J. S. Richardson, and D. C. Richardson. 2010. MolProbity: All-atom structure validation for macromolecular crystallography. *Acta Crystallogr. Sect. D Biol. Crystallogr.* **66**: 12–21.

43. The PyMol Molecular Graphics System, Version 1.8, Schrodinger, LLC.

44. Bourquin, F., H. Riezman, G. Capitani, and M. G. Grütter. 2010. Structure and function of sphingosine-1-phosphate lyase, a key enzyme of sphingolipid metabolism. *Structure*. **18**: 1054–1065.

45. Haraga, A., T. E. West, M. J. Brittnacher, S. J. Skerrett, and S. I. Miller. 2008. *Burkholderia thailandensis* as a model system for the study of the virulence-associated type III secretion system of burkholderia pseudomallei. *Infect. Immun.* **76**: 5402–5411.

46. Lloyd, M. D., K. D. E. Boardman, A. Smith, D. M. van Den Brink, R. J. A. Wanders, and M. D. Threadgill. 2007. Characterisation of recombinant human fatty aldehyde dehydrogenase: implications for Sjögren-Larsson syndrome. *J. Enzyme Inhib. Med. Chem.* **22**: 584–590.

47. Obeid, L. M., Y. Okamoto, and C. Mao. 2002. Yeast sphingolipids: Metabolism and biology. *Biochim. Biophys. Acta - Mol. Cell Biol. Lipids*. **1585**: 163–171.

48. Backhed, F., R. E. Ley, J. L. Sonnenburg, D. A. Peterson, and J. I. Gordon. 2005. Host-Bacterial Mutualism in the Human Intestine. *Science* **307**: 1915–1920.

49. Schweizer, H. P.. 2012. Mechanisms of antibiotic resistance in *Burkholderia pseudomallei*: implications for treatment of melioidosis Herbert P Schweizer. *Future Microbiol.* **7**: 1389–1399.

50. Mahenthiralingam, E., T. A. Urban, and J. B. Goldberg. 2005. The multifarious, multireplicon *Burkholderia cepacia* complex. *Nat. Rev. Microbiol.* **3**: 144–156.

51. Vandamme, P, J. Govan, and J. LiPuma. 2007. Diversity and Role of Burkholderia spp. *In* Burkholderia: Molecular Microbiology and Genomics. T. Coenyne and P. Vandamme, Horizon Bioscience, 1–28.

52. Stoffel, W. Lekim, D. Sticht, G.. 1969. Distribution and properties of dihydrosphingosine-1-phosphate aldolase. *Hoppe-Seyler's Physio. Chem.* **350**: 1233–1241.

53. Suh, J. H., A. Eltanawy, A. Rangan, and J. D. Saba. 2016. A facile stable-isotope dilution method for determination of sphingosine phosphate lyase activity. *Chem. Phys. Lipids*. **194**: 101–109.

54. Keller, M. A., U. Zander, J. E. Fuchs, C. Kreutz, K. Watschinger, T. Mueller, G. Golderer, K. R. Liedl, M.

Ralser, B. Kräutler, E. R. Werner, and J. A. Marquez. 2014. A gatekeeper helix determines the substrate specificity of Sjögren-Larsson Syndrome enzyme fatty aldehyde dehydrogenase. *Nat. Commun.* **5**: 4439.

55. Christen P. and P. K. Mehta. 2001. From cofactor to enzymes. The molecular evolution of pyridoxal-5'-phosphate-dependent enzymes. *Chem. Rec.* **1**: 436–447.

56. Weiler, S., N. Braendlin, C. Beerli, C. Bergsdorf, A. Schubart, H. Srinivas, B. Oberhauser, and A. Billich. 2014. Orally Active 7-Substituted (4-Benzyl-phthalazin-1-yl)-2-methyl-piperazin-1-yl]-nicotinonitriles as Active-site Inhibitors of Sphingosine-1-Phosphate Lyase for the Treatment of Multiple Sclerosis. *J. Med. Chem.* **57**: 5074–5084.

57. Rolando, M., P. Escoll, T. Nora, J. Botti, V. Boitez, C. Bedia, C. Daniels, G. Abraham, P. J. Stogios, T. Skarina, C. Christophe, D. Dervins-Ravault, C. Cazalet, H. Hilbi, T. W. T. Rupasinghe, D. Tull, M. J. McConville, S. Y. Ong, E. L. Hartland, P. Codogno, T. Levade, T. Naderer, A. Savchenko, and C. Buchrieser. 2016. *Legionella pneumophila* S1P-lyase targets host sphingolipid metabolism and restrains autophagy. *Proc. Natl. Acad. Sci. U. S. A.* **113**: 1901–1906.

58. Wadsworth, J. M., D. J. Clarke, S. A. Mcmahon, J. P. Lowther, A. E. Beattie, P. R. R. Langridge-Smith, H. B. Broughton, T. M. Dunn, J. H. Naismith, and D. J. Campopiano. 2013. The chemical basis of serine palmitoyltransferase inhibition by myriocin. *J. Am. Chem. Soc.* **135**: 14276–14285.

59. Dinges, J., C. M. Harris, G. A. Wallace, M. A. Argiriadi, K. L. Queeney, D. C. Perron, E. Dominguez, T. Kebede, K. E. Desino, H. Patel, and A. Vasudevan. 2016. Hit-to-lead evaluation of a novel class of sphingosine 1-phosphate lyase inhibitors. *Bioorganic Med. Chem. Lett.* **26**: 2297–2302.

60. Jones, A. L., T. J. Beveridge, and D. E. Woods. 1996. Intracellular survival of *Burkholderia pseudomallei*. *Infect.Immun.* **64**: 782–790.

61. Wand, M. E., C. M. Müller, R. W. Titball, and S. L. Michell. 2011. Macrophage and Galleria mellonella infection models reflect the virulence of naturally occurring isolates of *B. pseudomallei*, *B. thailandensis* and *B. oklahomensis*. *BMC Microbiol.* **11**: 11.

62. Hannun, Y. A. 1996. Functions of ceramide in coordinating cellular responses to stress. *Science*. **274**: 1855–1859.

63. Young, M. M., M. Kester, and H.-G. Wang. 2013. Sphingolipids: regulators of crosstalk between apoptosis and autophagy. *J. Lipid Res.* **54**: 5–19.

Enzyme		FALDH	S1PL2021	S1PL2025
Substrate		2E-HEX	S1P	S1P
V_{MAX}	(nanomoles/min/mg)	314.9 ± 13.9	17.5 ± 1.3	8.2± 1.775
K_M	(μM)	19.4 ± 3.2	48.2 ± 9.4	50.19 ± 8.3
k_{cat}	(s^{-1})	0.22 ± 0.01	0.015 ± 0.003	0.008 ± 0.0005
k_{cat}/K_M	($M^{-1}s^{-1}$)	1.13 x 10^4	3.2 x 10^2	1.5 x 10^2

Table 1. Michaelis Menten kinetic data for recombinant human FALDH using 2E-HEX as substrate and the *B. pseudomallei* S1PL2021 and S1PL2025 enzymes using S1P as a substrate.

Wavelength	0.976
Resolution range	43.27 - 2.104 (2.179 - 2.104)
Space group	P 1 2_1 1
Unit cell	59.6 126.776 59.725 90 97.508 90
Total reflections	280513 (25538)
Unique reflections	50729 (4971)
Multiplicity	5.5 (5.1)
Completeness (%)	1.00 (0.98)
Mean I/sigma(I)	8.57 (1.87)
Wilson B-factor	32.55
R-merge	0.1336 (0.6925)
R-meas	0.1475 (0.7717)
CC1/2	0.994 (0.671)
CC*	0.999 (0.896)
Reflections used in refinement	50714 (4970)
Reflections used for R-free	2637 (273)
R-work	0.1688 (0.2445)
R-free	0.2268 (0.3101)
CC(work)	0.947 (0.834)
CC(free)	0.932 (0.743)
Number of non-hydrogen atoms	7190
macromolecules	6890
Protein residues	879
RMS(bonds)	0.013
RMS(angles)	1.22
Ramachandran favored (%)	97
Ramachandran allowed (%)	2.9
Ramachandran outliers (%)	0
Rotamer outliers (%)	1.8
Clashscore	3.26
Average B-factor	39.12
macromolecules	39.17
solvent	37.96

Table 2. S1PL2021 X-ray crystallographic data collection and refinement statistics.

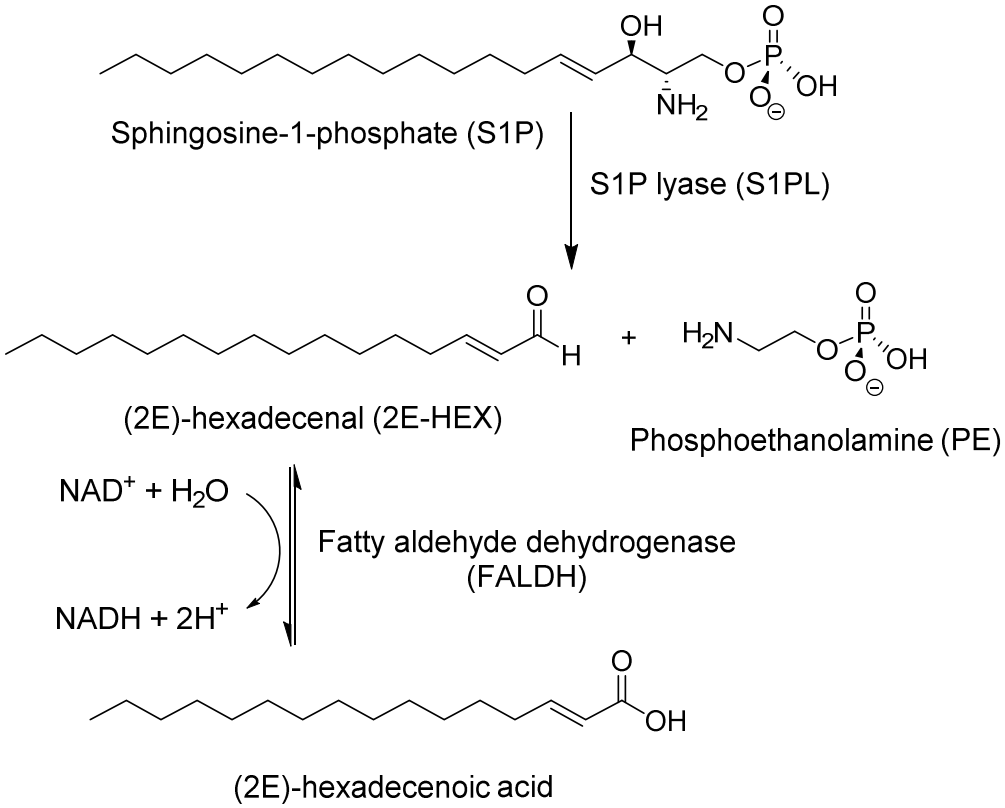

Fig. 1. Metabolism of sphingosine 1-phosphate (S1P). Sphingosine 1-phosphate lyase (S1PL) catalyses the degradation of S1P to (2E)-hexadecenal (2E-HEX) and phosphoethanolamine (PE).The 2E-HEX product is a substrate for the NAD^+-dependent enzyme, fatty aldehyde dehydrogenase (FALDH), which oxidizes 2E-HEX to the fatty acid with the concomitant reduction of the NAD^+ cofactor.

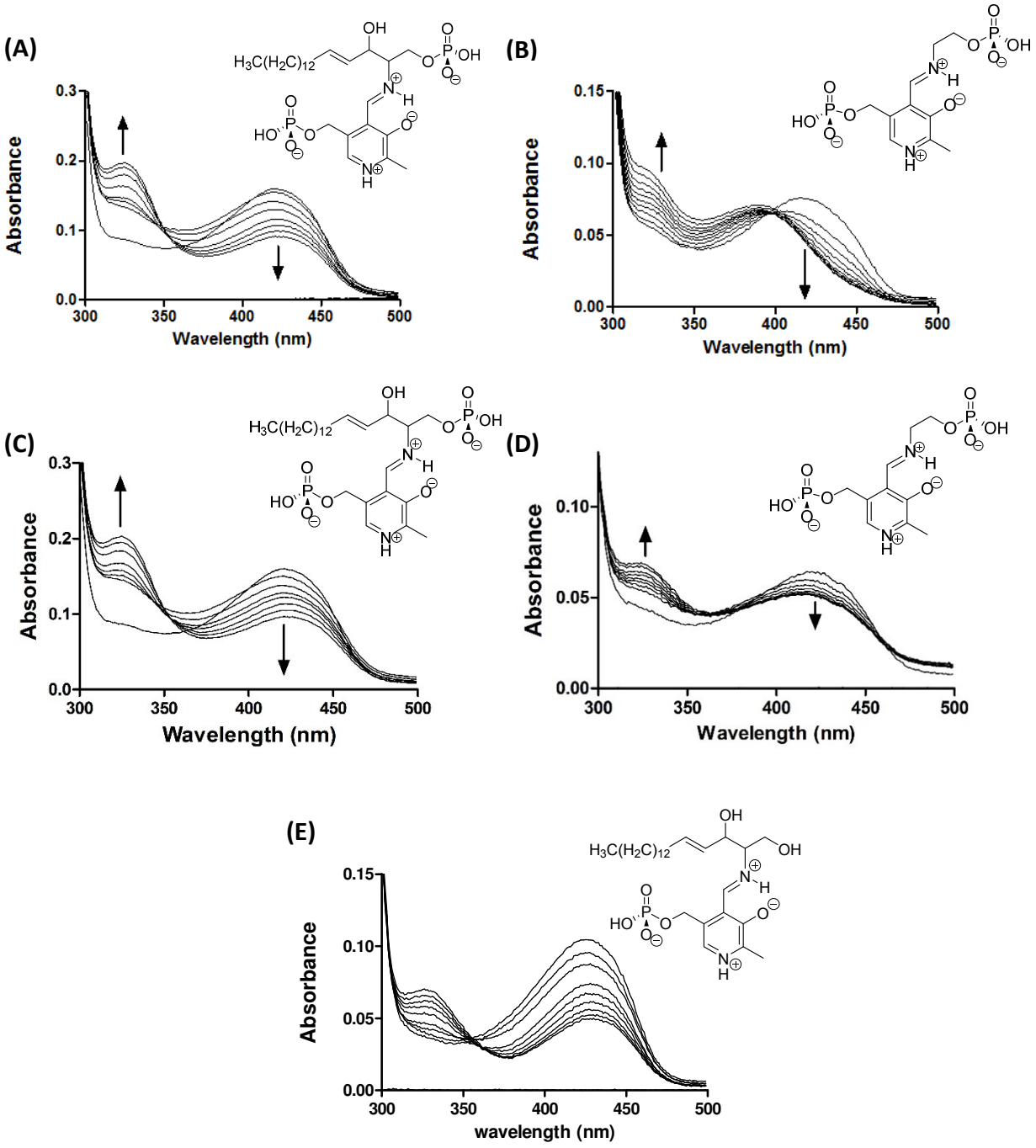

Fig. 2. UV-visible spectroscopy analysis of purified S1PL2021. (A) The UV-vis spectrum of PLP-bound S1PL2021 changes upon incubation with 100 µM S1P substrate in a time-dependent manner. Over 30 mins (scanning every 5 mins), a decrease in absorbance at 420 nm, coupled to an increase in the 330 nm region is observed. The structure of the PLP-S1P external aldimine substrate is shown. **(B)** Addition of 10 mM PE to S1PL2021 results in changes to the PLP spectrum over a longer timeframe (3 hrs, scanning every 30 mins). There is a shift of the 420nm peak to 395 nm and a broader increase in the 320-380 nm region associated with the formation of PLP-PE external aldimine (structure shown). **(C)** Addition of 100 µM S1P to S1PL2025 leads

to changes in the PLP UV-vis spectrum region similar to that observed with S1PL2021 (30, with scans every 5 mins) **(D)** Addition of 10 mM PE to S1PL2025 results in changes to the PLP spectrum over a longer timeframe (3 hrs, scanning every 30 mins). (**E**) Addition of 300 μM D-*erythro* sphingosine to S1PL2021 results in changes to the PLP spectrum (4 hrs, scanning every 30 mins).

JOURNAL OF LIPID RESEARCH

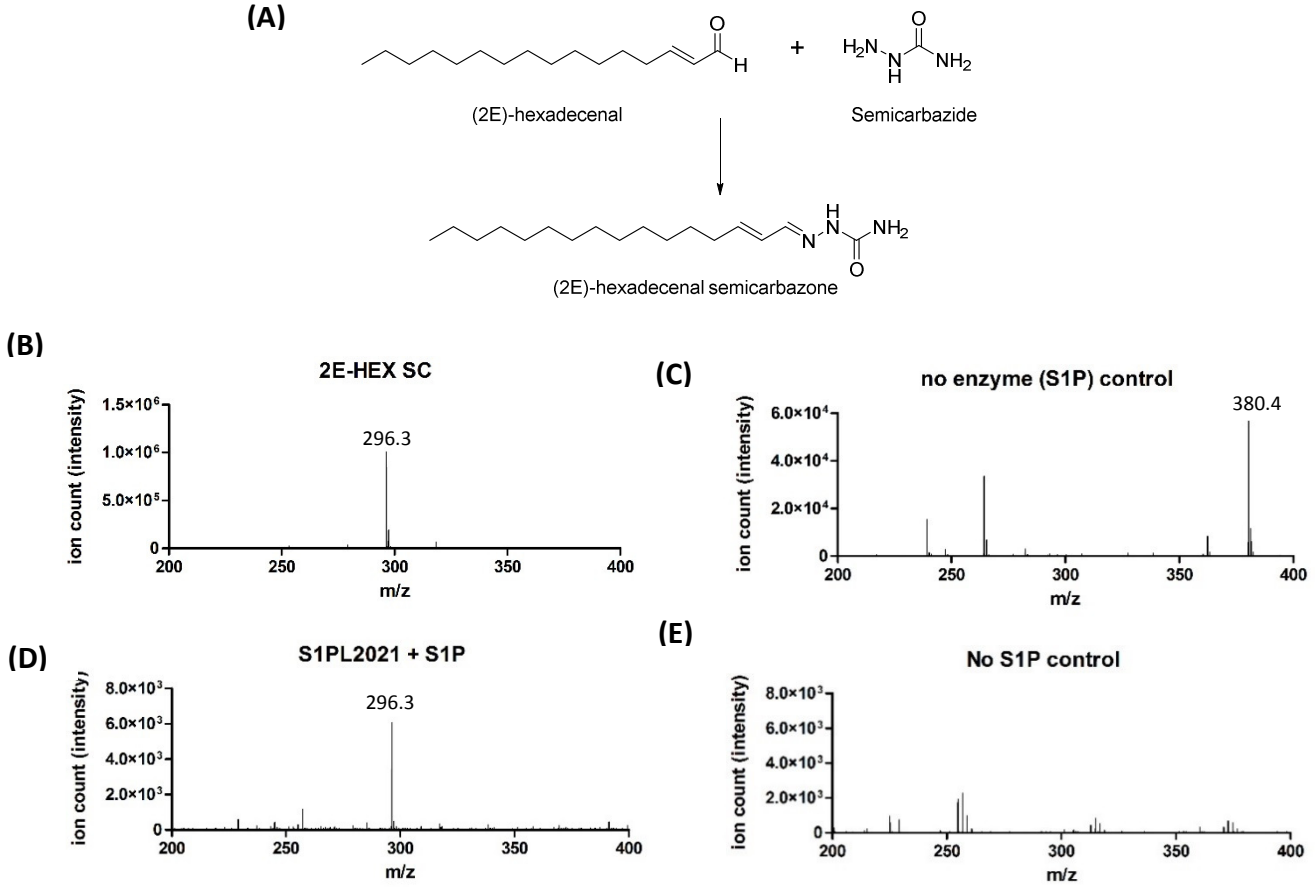

Fig. 3. Analysis of S1PL2021 activity by the Berdyshev *et al* method. (**A**) The reaction between 2E-HEX and semicarbazide leads to formation of the semicarbazone derivative (2E-HEX SC) which under ESI-MS gives an ion with predicted value of *m/z* = 296.3 Da ($[M+H]^+$, $C_{17}H_{34}N_3O^+$). (**B**) ESI-MS analysis of the 2E-HEX positive control reaction showing an ion with *m/z* = 296.3 Da corresponding to the 2E-HEX SC. (**C**) Incubation of S1P in buffer followed by semicarbazide derivitisation in the absence of enzyme. The ion with *m/z* = 296.3 Da is absent but an ion with *m/z* = 380.4 Da corresponding to S1P is observed ($[M+H]^+$, $C_{18}H_{38}NO_5P$ = 380.2 Da, predicted). (**D**) The S1PL2021 enzymatic reaction showing the formation of the 2E-HEX SC ion with *m/z* = 296.3 Da confirming the activity of S1PL2021. (E) The no substrate control lacking S1P and the 2E-HEX SC.

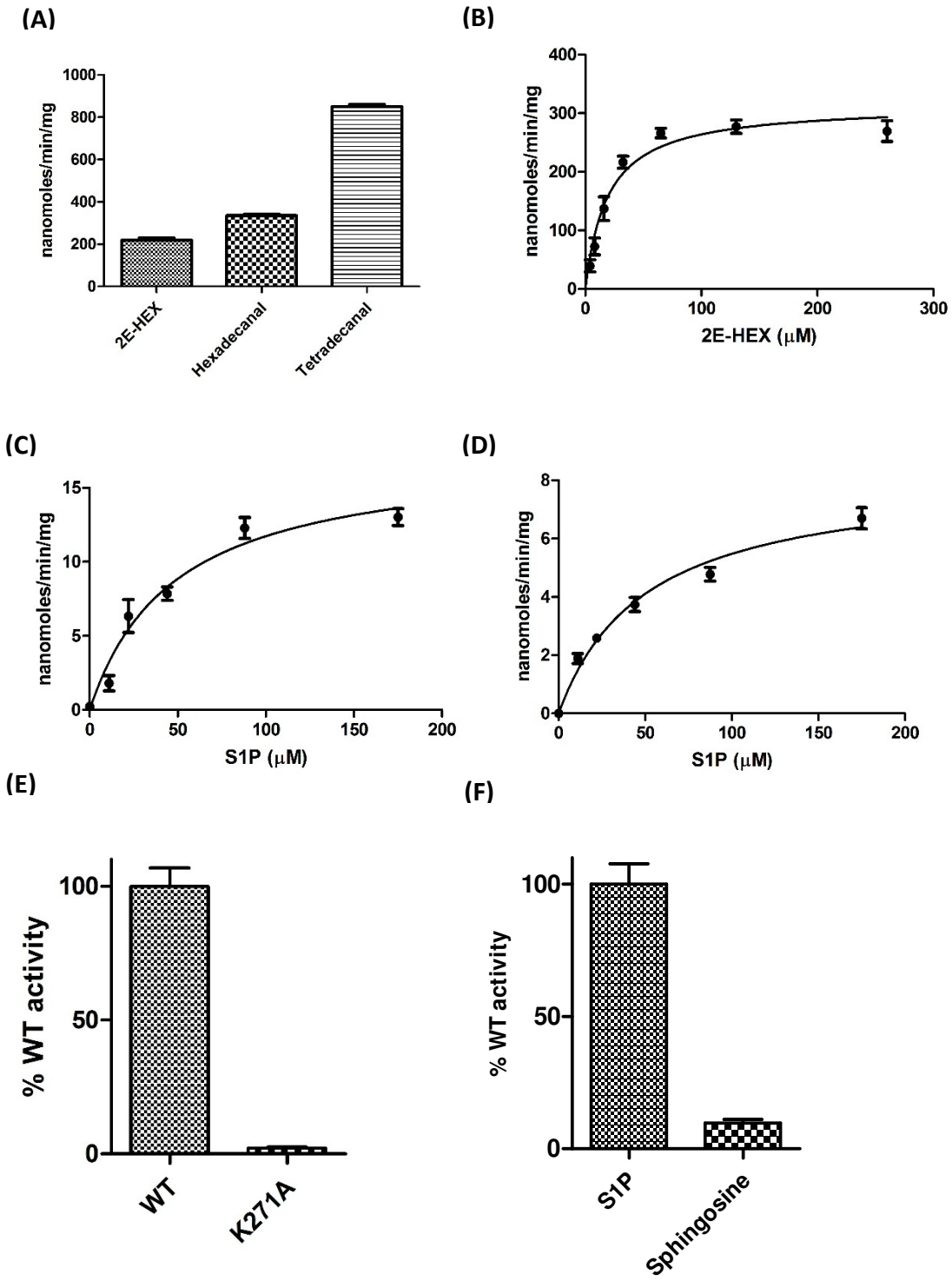

Fig. 4. Kinetic analysis of FALDH and S1PL2021/S1PL2025. (A) Recombinant human FALDH (0.5 μM) displays enzyme activity with aldehyde substrates 2E-HEX, hexadecanal and tetradecanal. **(B)** Michaelis Menten kinetic analysis of FALDH using 2E-HEX as a substrate (0-260 μM). The K_M for 2E-HEX = 19.4 ± 3.2 μM and k_{cat} = 0.22 ± 0.01 s^{-1}. **(C and D)** Michaelis Menten kinetic analysis using the S1PL/FALDH coupled assays with S1P as substrate (6.0 μM S1PL, 0.5 μM FALDH). The K_M and k_{cat} values for S1P are; 48.2 ± 9.4 μM and 0.015 ± 0.003s^{-1} for (**C**) S1PL2021, and 50.2 ± 8.3 μM and

$0.008 \pm 0.0005 s^{-1}$ for (**D**) S1PL2025. **(E)** The S1PL2021 K271A mutant displays negligible activity when using the coupled assay. (**F**) Use of the coupled assay to allow comparison of the S1PL20121 lyase activity with S1P (100 μM) and D-*erythro* sphingosine (300 μM) substrates.

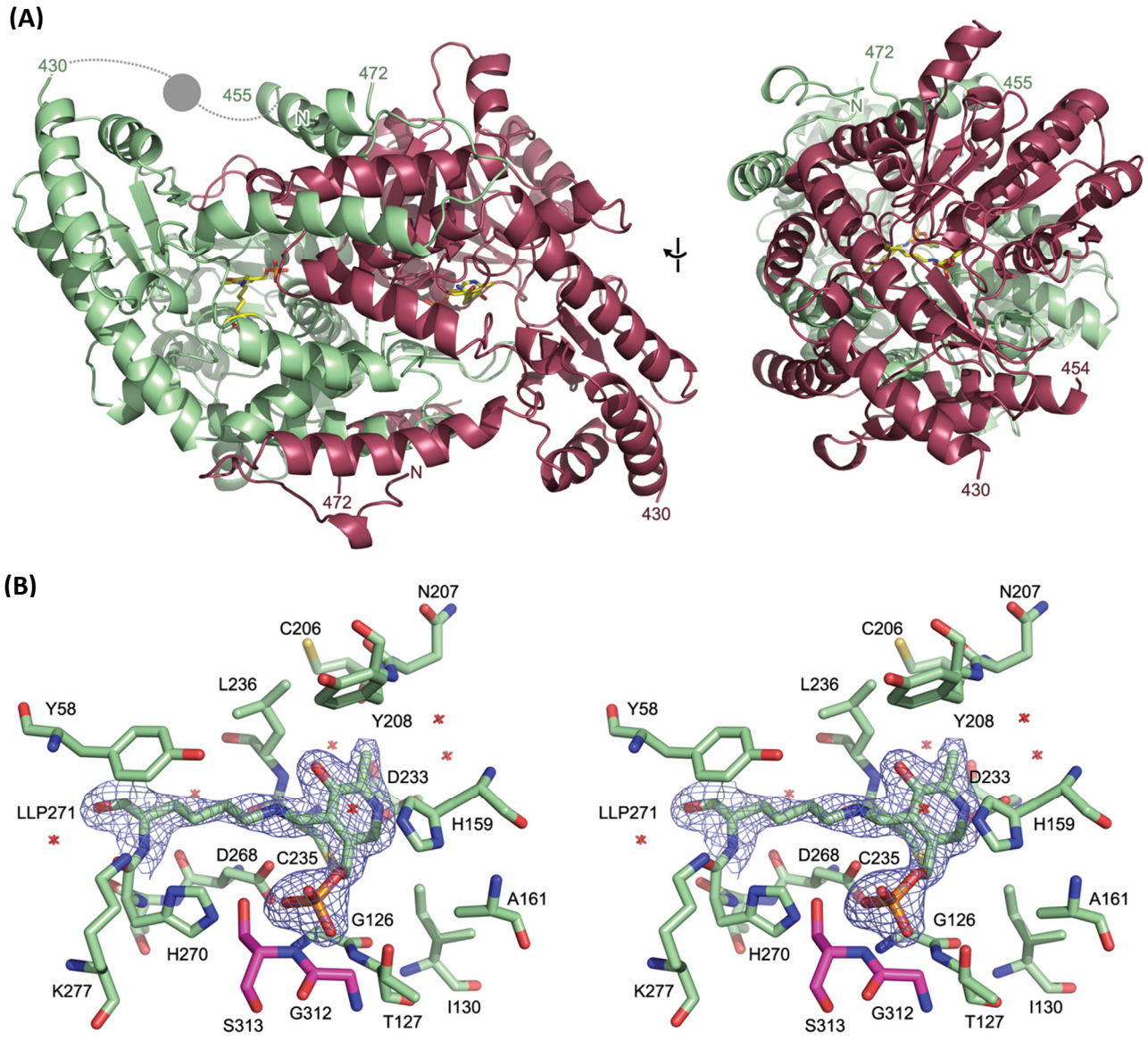

Fig. 5. Structure of S1PL2021. (**A**) Orthogonal views of the secondary structure of the S1PL2021 homodimer (PDB code: 5K1R). The two chains present in the asymmetric unit are shown as cartoon representations in green and red. The PLP cofactor bound as an internal aldimine to K271 is shown as sticks (LLP271). The region of the protein between residues 430 and 455 that was absent from the experimental electron density is modelled based on homologous structures; the dashed lines represent loops and circle represents an alpha helix. (**B**) Stereo view of the PLP-binding site of S1PL2021. Residues within 4 Å of the PLP cofactor are shown as sticks. Water molecules in this site are shown as crosses. The experimental 2mFo-DFc electron density is shown contoured at 1.5 σ around the internal aldimine formed between the PLP and K271 (LLP271). The PLP binding site is at the dimer interface and residues from each monomer are coloured green and red.